

External Measurements and Visceral Response in a Cross-Sectional Torso Impact Model

J. J. Hallman, N. Yoganandan, F. A. Pintar

Department of Neurosurgery, Medical College of Wisconsin

This paper has not been screened for accuracy nor refereed by any body of scientific peers and should not be referenced in the open literature.

ABSTRACT

Post-mortem human specimen (PMHS) experiments have correlated torso biomechanics (e.g., deflection and VC) to injury risk using the chestband, an instrumented flexible steel belt. From the chestband, time dependent contours are derived representing torso cross-sectional shape throughout the impact event. Biomechanical injury metrics are typically computed from uniaxial measurements between two contour points in order to develop metrics for uniaxial transducers within anthropomorphic test devices (ATDs). Yet, the relationship between uniaxial deformation measurements and the underlying tissue response in humans is not well understood. Prior PMHS experiments have suggested a causative relationship between localized posterolateral thorax loading and regional visceral injury, but sample size has precluded development of injury metrics specific to this loading direction. Therefore, a plane strain viscoelastic finite element model was employed to correlate posterolateral uniaxial deformations, i.e., deflection and VCmax, with visceral (spleen) strain and strain energy density responses. Model visceral geometry was also varied to simulate small, median, and large visceral volumes across the American population. The model was exercised by applying normalized subject-specific chestband deformations to the model periphery; material responses throughout the spleen were determined. Considering all simulations, Coefficients of Determination (R^2) and the Predicted Sum of Squares (PRESS) were computed to quantify correlations between visceral responses (i.e., parenchymal strain, capsular strain, and strain energy density) and external metrics (i.e., deflection and VCmax) measured between 90° and 140° with respect to the anterior direction. PRESS and R^2 statistics were determined for 3 visceral anatomic variants, 11 angles, 2 metrics, and 3 visceral response parameters, totaling 198 analyses. Correlations at 140° were not significant for any metric or anatomic variant. Generally deflection was a better predictor of visceral response than VCmax; peak R^2 values occurred at 125° (capsular

strain), 115° (parenchymal strain), and 90° (strain energy density). Because the loading set was composed of only ten experiments, the PRESS statistic determined the degree to which analyses were generalizable to a larger population. PRESS results indicated that deflection was a more generalizable metric than VCmax and that angles 115 – 125° were associated with greatest correlations. These results suggested that, to measure visceral injury risk, an ATD transducer would be appropriately located between 115° and 125° within the thorax. This model formulation is useful for parametric examination of visceral response to torso deformations measured experimentally using the chestband device.

INTRODUCTION

The chestband device consists of a flexible steel belt instrumented with resistive strain gages in an axially-compensated Wheatstone bridge configuration (Eppinger, 1989). Bridge outputs, representing band curvature at underlying points, are post-processed with cubic spline interpolation into two-dimensional (2D) closed contours for each sample time. The post-processing algorithm RBandPC (ver. 3.0, Conrad Technologies, Inc., Washington DC, available from the US Department of Transportation) was validated using an anthropomorphic test device in sled impacts (Pintar et al., 1996). During blunt lateral impact to the thorax and abdomen, external deflection from the chestband has been identified as a correlate to resulting injury (Pintar et al., 1997) and comparable or superior to deflections obtained from depth-limited impactors (Chung et al., 1999), from post-experiment digitization of videography (Viano et al., 1989), and from invasive linear displacement transducers (Kemper et al., 2008).

Recent lateral impact studies with the chestband have identified complex multidirectional deformation patterns induced by narrow object vehicle intrusion (Yoganandan et al., 2008) or seat-mounted torso side airbag interaction (Hallman et al., 2010). These deformations likely pose injury risk to underlying structures but a uniaxial measurement direction is less apparent from experimental data (Kuppa et al., 2003). In particular, PMHS experiments with side airbag suggested postero-lateral interaction may induce trauma to viscera, but traditional lateral deformation measurements did not capture fully the thorax biomechanical response to this boundary condition (Hallman et al., 2010). Consequently, a planar viscoelastic finite element (FE) model was developed to study the relationship between these complex external deformation patterns and internal tissue viscoelastic response (Hallman et al., 2011b).

Previously, this planar FE model was employed to quantify visceral strain and strain energy density responses to 2D chestband contours from PMHS experiments. In that study, the model was exercised by applying to the periphery 21 subject-specific PMHS chestband deformation patterns representing four boundary conditions: (a) lateral impact with close-proximity torso airbag, (b) stationary close-proximity torso airbag loading, (c) flat rigid lateral impact, and (d) antero-lateral oblique rigid impact. ANOVA determined that mean peak material responses were correlated to boundary condition ($p < 0.002$). Using matched-pair experiment injury outcomes, risk of visceral trauma corresponded to localized strain and strain energy density ($p < 0.1$).

To translate FE results to ATD design direction, the present study coupled this planar FE model with chestband contours exhibiting deformations in the posterolateral region of the thorax and abdomen. Uniaxial measurements in the posterolateral region were obtained from multiple angles with respect to the anterior direction. Statistical analysis was completed to identify measurements most correlated to viscoelastic response in the underlying viscera.

METHODS

The FE model employed in this study has been described elsewhere (Hallman et al., 2011b). The development and validation processes are summarized here for reference only. Further details are available in the literature. The FE model was developed from imaging data produced by the Visible Human Project (National Library of Medicine, National Institutes of Health, Bethesda, MD). An image corresponding to the T1 vertebral body level was selected to represent model geometry with the following structures: vertebral body, chest wall, sternum, liver, spleen, omentum and hollow intra-abdominal structures, and external “flesh” tissue.

Freeform curve geometries were then rendered with defined lines and arcs. The geometry was discretized into 11,438 elements (Fig. 1), 91.1% of which were characterized by aspect ratios < 2; 99.3% of element quadratic angles were between 45° and 135°. Self-contacts were defined between all nodes to prevent self-penetration. Frictionless surface-to-surface contacts were defined between all intra-abdominal contents and the chest wall.

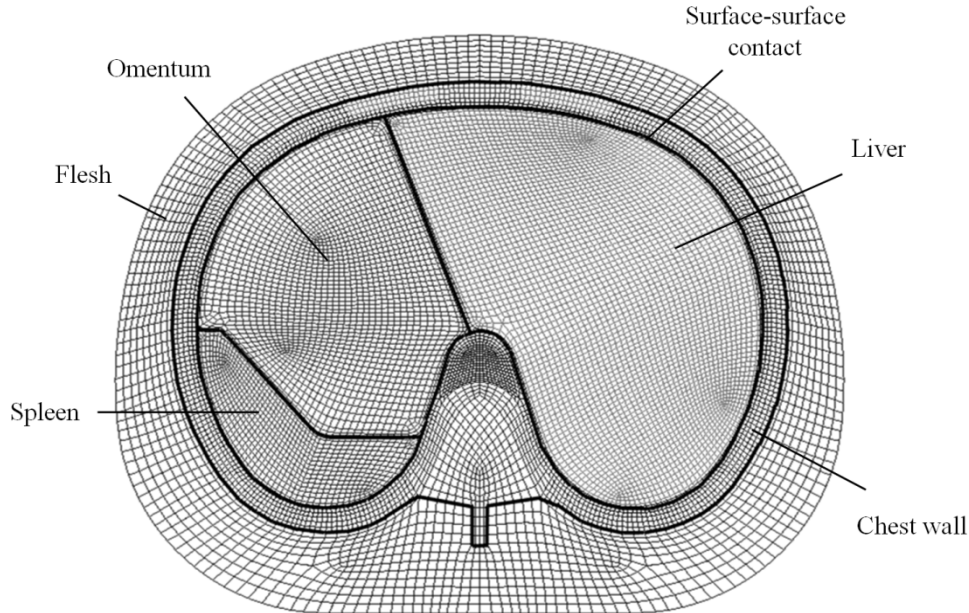


Figure 1. Mesh density for the median planar model.

Geometric Variations

Two anatomic variants were considered to identify any geometric dependencies between external biomechanical parameters and material responses. Visceral volumes follow a normal distribution when corrected for subject gender and standardized height and weight (Geraghty et al., 2004) according to Eq. 1:

$$V_{\text{corrected}} = V_{\text{measured}} + F_{\text{ht}} \times (H_{\text{std}} - H_j) + F_{\text{wt}} \times (W_{\text{std}} - W_j) \quad \text{Eq. 1}$$

V corresponds to organ volume, H_j and W_j are height and weight for subject j, H_{std} and W_{std} are standardized height and weight, and F_{wt} and F_{ht} are correction coefficients determined by the study. The standardized 50th percentile male anthropometry represents $H_{\text{std}} = 1.76$ m and $W_{\text{std}} = 73.0$ kg. The Visible Male was determined to contain a 33rd percentile liver and a 47th percentile spleen in the 2D model. By assuming that organ dimensional changes occur proportionally in three dimensions, cross-sectional areas were scaled to the 50th percentile (median) male according to Eq. 2:

$$A_{\text{corrected}} = A_{\text{measured}} \times (V_{\text{corrected}} / V_{\text{measured}})^{2/3} \quad \text{Eq. 2}$$

where A represents organ cross-sectional area and V represents organ volume. Using Eqs. 1 and 2, two additional models were developed from the initial model with visceral geometries coinciding with the human 5th percentile (small) and 95th percentile (large) liver and spleen volumes (Fig. 2). These anatomic variant models were meshed similarly to the median model. The small variant model was composed of 11,382 elements, 90.0% of which were characterized by aspect ratios less than 2. No less than 98.5% of element quadratic angles were between 45° and 135°. The large variant model was composed of 11,680 elements, 90.9% of which were characterized by aspect ratios less than 2. No less than 98.6% of element quadratic angles were between 45° and 135°.

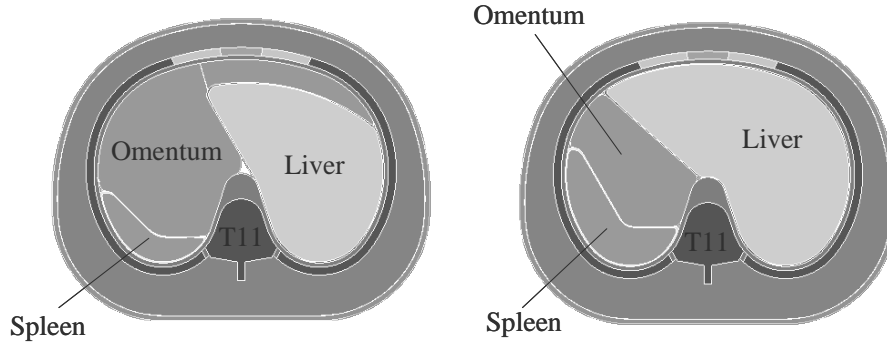


Figure 2. Anatomic variant model variations corresponding to small (left) and large (right) visceral contents.

Material Properties

Material properties remained unchanged from the previous model (Hallman et al., 2011b). For reference, these were selected according to the literature and from iterative tuning to published biomechanical experiments (Seki & Iwamoto, 1998; Carter et al., 2001; Stingl et al., 2002; Tamura et al., 2002; Behr et al., 2003; Ruan et al., 2003). Material models were assumed as follows: The vertebral body and sternum, rigid; the chest wall, costal cartilage, and costovertebral tissues, linear elastic; subcutaneous flesh, liver, spleen, diaphragm, and omentum, linear viscoelastic. Final properties are given in Table 1 and were identical between the three model geometries.

Table 1. Material properties chosen for the planar torso model.

Material	ρ (kg/m^3)	K/E (MPa)	G_0 (MPa)	G_∞ (MPa)	Poisson ratio
Flesh	1100	0.5	0.350	0.170	
Chest Wall	1310	350	-	-	0.3
Costal Cartilage	1200	25	-	-	0.4
Costovertebral Junction	1200	50	-	-	0.4
Omentum	1100	0.5	0.054	0.040	-
Diaphragm	1100	0.5	0.400	0.100	-
Liver: Parenchyma	1100	0.5	0.230	0.044	-
Liver: Capsule	1100	-	0.300	0.065	-
Spleen: Parenchyma	1100	0.5	0.069	0.013	-
Spleen: Capsule	1100	-	0.345	0.065	-

Loading

The model was exercised with displacement-driven loading definitions using xyphoid-level chestband results from PMHS experiments. Because initial chestband contours were subject-specific due to differing anthropometry, e.g., chest depth and breadth, contours were systematically scaled to the model geometry using a customized mapping algorithm (Hallman et al., 2011a). Surface-to-surface contact without sliding was defined between the FE chestband and the model flesh.

Two boundary conditions involving torso side airbag loading were selected to represent multidirectional deformation patterns involving lateral and posterior aspects of the left hemithorax. These left-side sled impacts consisted of (a) close-proximity side airbag contact with sled $\Delta V = 6.7$ m/s, $n = 4$ and (b) close-proximity side airbag contact with stationary subject, $n = 3 \times 2$ aspects (Hallman et al., 2010). For stationary airbag contact, three PMHS were subjected to both right and left aspect loading; right-side experiment datasets were inverted about the SAE x-axis to model left-sided loading. To maintain realistic inertial response, a planar acceleration field was applied to the model nodes as obtained from accelerometers mounted to the T12 spinous process during each PMHS experiment.

Output Parameters

Material response was examined in the FE spleen, the left posterolateral visceral organ of this model. Three response parameters were investigated: Strain energy density (NRG), capsular principal strain (ϵ_C), and parenchymal principal strain (ϵ_I). From each simulation, the locations of peak NRG, peak ϵ_C , and peak ϵ_I were obtained. A contiguous area encompassing the peak response element and equal to 5% of total spleen cross-sectional area was identified; maximum response was considered to be the average material response obtained from this area at the instant the peak was obtained. Biomechanical parameters of peak normalized deflection and VCmax were quantified at eleven angles ($\theta = 90^\circ - 140^\circ$) with respect to the spine-sternum line (Fig. 3). The significance, Coefficient of Determination (R^2), and the Predicted Sum of Squares (PRESS) statistic were computed to assess the relationship between peak responses (NRG, ϵ_C , and ϵ_I) and external biomechanical response parameters. The R^2 is bounded by [0 1] and represented the proportion of material response variance for which the biomechanical parameter is predictive. The PRESS statistic quantified the degree to which the resulting regression may be generalized to a larger dataset; lower values indicate better generalizability.

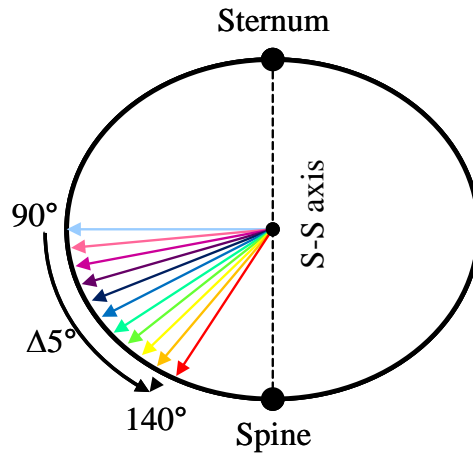


Figure 3. Measurement vectors evaluated for correlation to internal material response parameters.

RESULTS

Shown in Figure 4 are exemplar images of deformation response to two boundary conditions representing (a) side airbag with $\Delta V = 6.7$ m/s and (b) side airbag with stationary subject. Contained in Table 2 are the significance values from a correlation matrix between maximum material responses and peak posterolateral metrics of normalized deflection and VCmax. Correlations were not significant at $\theta = 140^\circ$ for any geometry or at $\theta = 135^\circ$ for small viscera geometry. Further, strain energy density appeared least correlated with posterolateral biomechanics; results were significant only at $\theta \leq 120^\circ$ (115° for the small viscera geometry).

Shown in Figures 5-7 are R^2 values overlaid with corresponding PRESS statistics for all material responses evaluated in this analysis. Recall that the R^2 value represents the proportion of material response variance for which the biomechanical parameter is predictive. Recall that the PRESS statistic quantifies the degree to which the resulting relationship may be generalized to a larger dataset. Therefore the best metric demonstrates maximal R^2 and minimal PRESS. In general, the angles yielding the lowest PRESS values were in agreement with the angles yielding the greatest R^2 values. Strain energy density (NRG) was least correlated with the external biomechanical parameters compared to ϵ_I and ϵ_C : Only for the large viscera geometry with normalized deflection at $\theta = 90^\circ - 100^\circ$ was $R^2 > 0.7$. By comparison, capsular strain indicated highest correlation to biomechanical metrics for the median and large viscera geometries; parenchymal strain indicated highest correlation only for the small viscera geometry.

With increased spleen size, PRESS and R^2 values indicated improved correlations. Highest overall R^2 values were observed for capsular and parenchymal strains in the large anatomic model between $\theta = 115^\circ - 125^\circ$ (Fig. 7). For this geometry, VCmax was preferable to normalized deflection. For median geometry (Figure 6), R^2

and PRESS values indicated normalized deflection was preferable to VCmax, but at angles similar to the large geometry. Comparatively, spleen material response in the small geometry did not correlate as well with external biomechanical metrics. Yet considering maximum parenchymal strain, $R^2 \approx 0.85$ for peak normalized deflection and VCmax at $\theta = 110^\circ$.

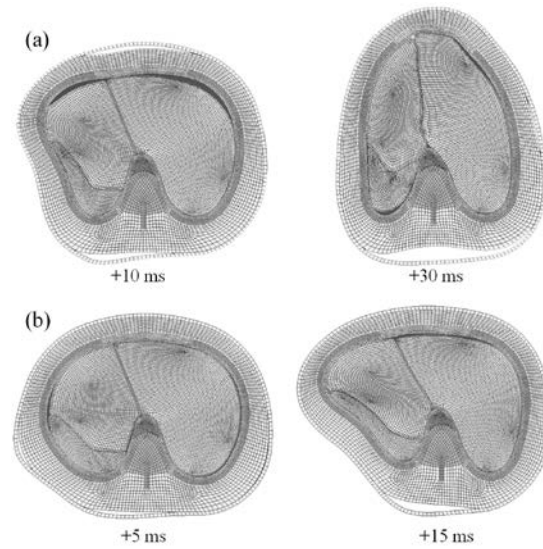


Figure 4. Exemplar median model response to (a) dynamic close-proximity airbag and (b) stationary close-proximity airbag.

DISCUSSION

This comparative subject-specific loading analysis demonstrated that tissue-level spleen responses are correlated with external thoracoabdominal biomechanics and visceral anatomic variations. Greatest correlation was found between angles $\theta = 115^\circ - 125^\circ$ with respect to the anterior direction. Increased size of viscera generally increased the level of correlation.

Model response was validated to individual organ/tissue experiments and to lateral and oblique PMHS pendulum impacts (Hallman et al., 2011b). Liver response was validated to dynamic compression tests of perfused whole primate livers at 2.5 s^{-1} (Melvin et al., 1973). Spleen response was validated to compression experiments of porcine splenic tissue at 0.5 s^{-1} (Tamura et al., 2002). Stress-strain and force-displacement results for liver and spleen simulations remained within corridors defined by the range of experimental data. The isolated chest wall geometry was validated to dynamic eviscerated PMHS chest compression experiments (Kent, 2008). Corridors were developed from linear fit results reported from PMHS experiments and model response fell within experimental variability. The complete model response was validated to lateral and oblique PMHS rigid pendulum impacts at 2.5 m/s, 4.5 m/s, and 6.5 m/s (Viano et al., 1989; Shaw et al., 2006). For whole model response, deflection was obtained from the relative translation between opposing peripheral subcutaneous nodes parallel to the impact direction. Force-deflection plots for pendulum impacts compared favorably with reported experimental results. Peak forces and peak deflections were within the ranges of peaks obtained from PMHS experiments.

Table 2. Correlation significance between oblique metrics and material response parameters for three anatomic variants.

5th Percentile (Small) Model						
Angle	NRG		ϵ_C		ϵ_1	
	NormD	VCmax	NormD	VCmax	NormD	VCmax
140 °	<i>0.864</i>	<i>0.633</i>	<i>0.180</i>	<i>0.109</i>	<i>0.870</i>	<i>0.643</i>
135 °	<i>0.773</i>	<i>0.314</i>	<i>0.062</i>	<i>0.055</i>	<i>0.389</i>	<i>0.151</i>
130 °	<i>0.396</i>	<i>0.223</i>	0.014	0.036	<i>0.089</i>	0.019
125 °	<i>0.193</i>	<i>0.230</i>	0.004	0.058	0.018	0.011
120 °	<i>0.070</i>	<i>0.163</i>	0.003	0.055	0.001	0.003
115 °	0.034	<i>0.056</i>	0.006	0.034	0.000	0.000
110 °	0.019	0.026	0.011	0.031	0.000	0.000
105 °	0.012	0.016	0.016	0.036	0.000	0.000
100 °	0.010	0.014	0.018	0.041	0.000	0.000
95 °	0.009	0.015	0.021	0.053	0.000	0.000
90 °	0.009	0.020	0.026	0.063	0.000	0.000
50th Percentile (Median) Model						
Angle	NRG		ϵ_C		ϵ_1	
	NormD	VCmax	NormD	VCmax	NormD	VCmax
140 °	<i>0.978</i>	<i>0.477</i>	<i>0.060</i>	<i>0.072</i>	<i>0.868</i>	<i>0.683</i>
135 °	<i>0.612</i>	<i>0.224</i>	0.006	0.008	<i>0.387</i>	0.203
130 °	<i>0.271</i>	<i>0.165</i>	0.000	0.000	<i>0.083</i>	0.038
125 °	<i>0.117</i>	<i>0.186</i>	0.000	0.000	0.015	0.026
120 °	0.036	<i>0.122</i>	0.000	0.001	0.001	0.008
115 °	0.015	0.038	0.002	0.003	0.000	0.002
110 °	0.008	0.017	0.010	0.009	0.000	0.001
105 °	0.005	0.012	0.023	0.017	0.000	0.001
100 °	0.004	0.011	0.031	0.023	0.000	0.002
95 °	0.003	0.012	0.043	0.031	0.000	0.003
90 °	0.003	0.016	0.058	0.034	0.000	0.005
95th Percentile (Large) Model						
Angle	NRG		ϵ_C		ϵ_1	
	NormD	VCmax	NormD	VCmax	NormD	VCmax
140 °	<i>0.868</i>	<i>0.401</i>	<i>0.177</i>	<i>0.170</i>	<i>0.481</i>	<i>0.291</i>
135 °	<i>0.508</i>	<i>0.183</i>	0.031	0.015	<i>0.141</i>	0.024
130 °	<i>0.200</i>	<i>0.133</i>	0.001	0.000	0.016	0.000
125 °	<i>0.077</i>	<i>0.158</i>	0.000	0.000	0.002	0.000
120 °	0.020	<i>0.100</i>	0.000	0.000	0.000	0.000
115 °	0.009	0.032	0.001	0.000	0.000	0.000
110 °	0.005	0.015	0.003	0.001	0.000	0.000
105 °	0.003	0.012	0.008	0.003	0.000	0.000
100 °	0.002	0.012	0.011	0.004	0.000	0.000
95 °	0.002	0.014	0.015	0.006	0.001	0.000
90 °	0.002	0.018	0.022	0.007	0.001	0.000

Values in italics are not significant.

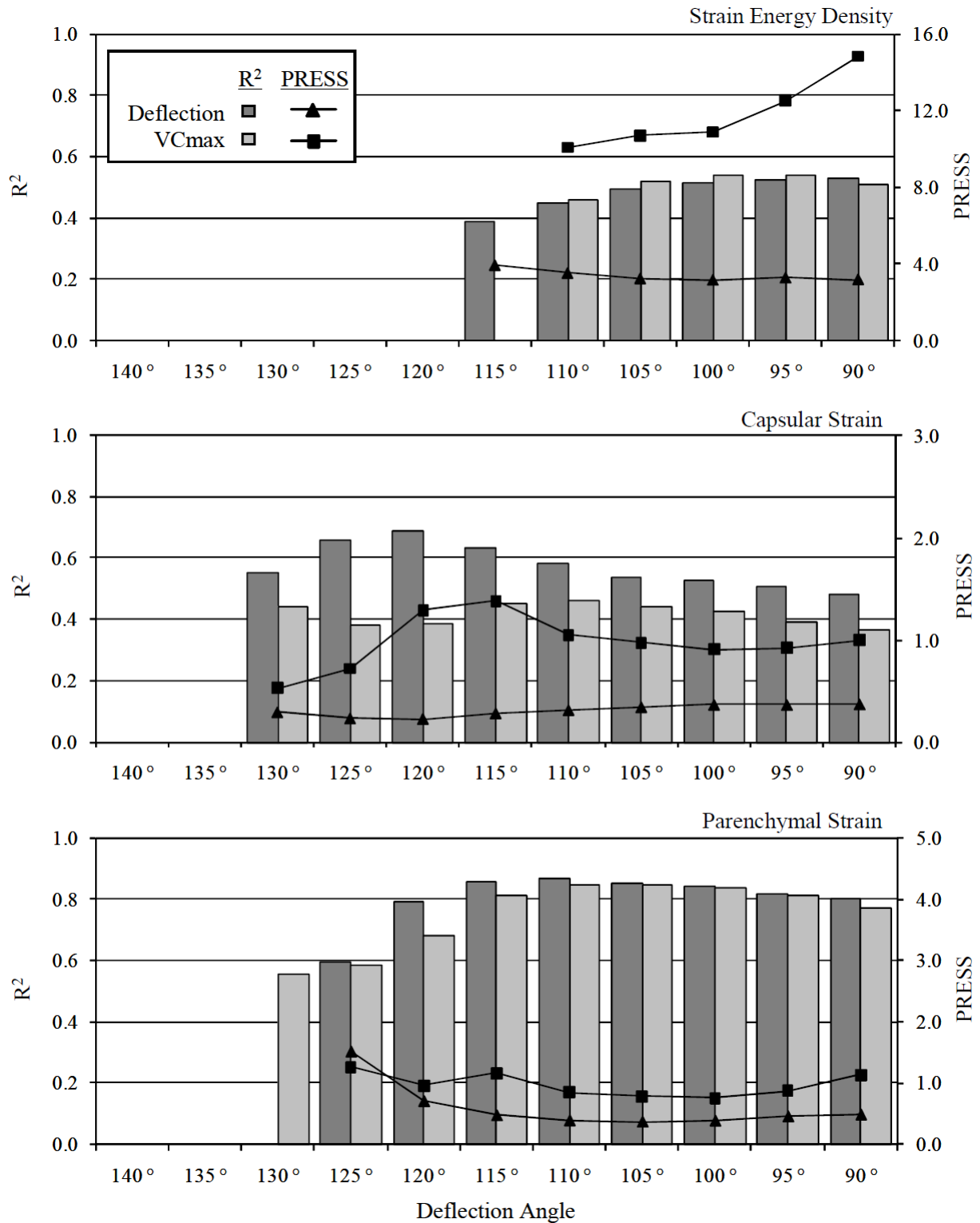


Figure 5. Coefficients of Determination (R^2) and PRESS statistics for correlations between oblique biomechanical parameters and tissue-level responses with small (5th percentile) viscera model.

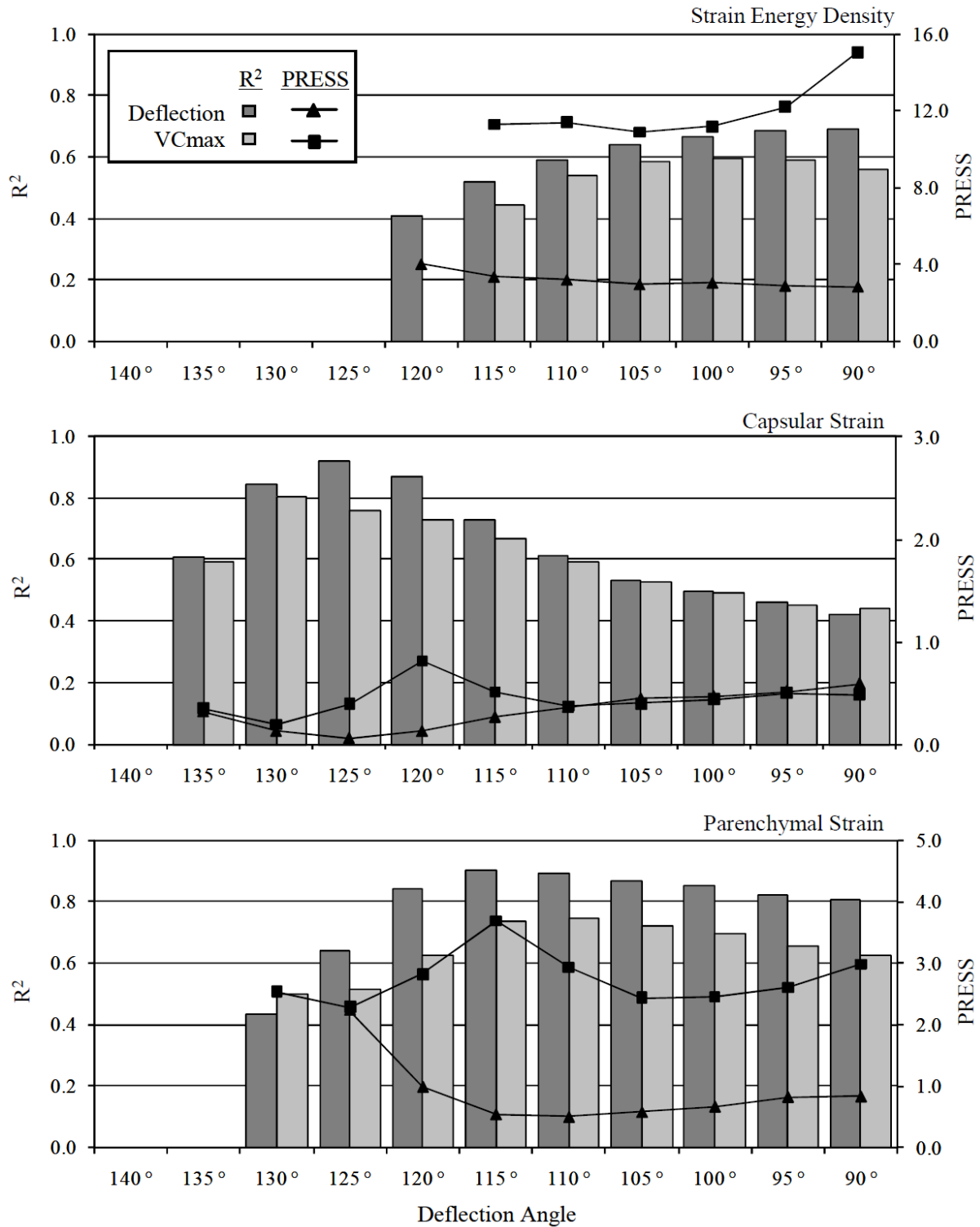


Figure 6. Coefficients of Determination (R^2) and PRESS statistics for correlations between oblique biomechanical parameters and tissue-level responses with median (50th percentile) viscera model.

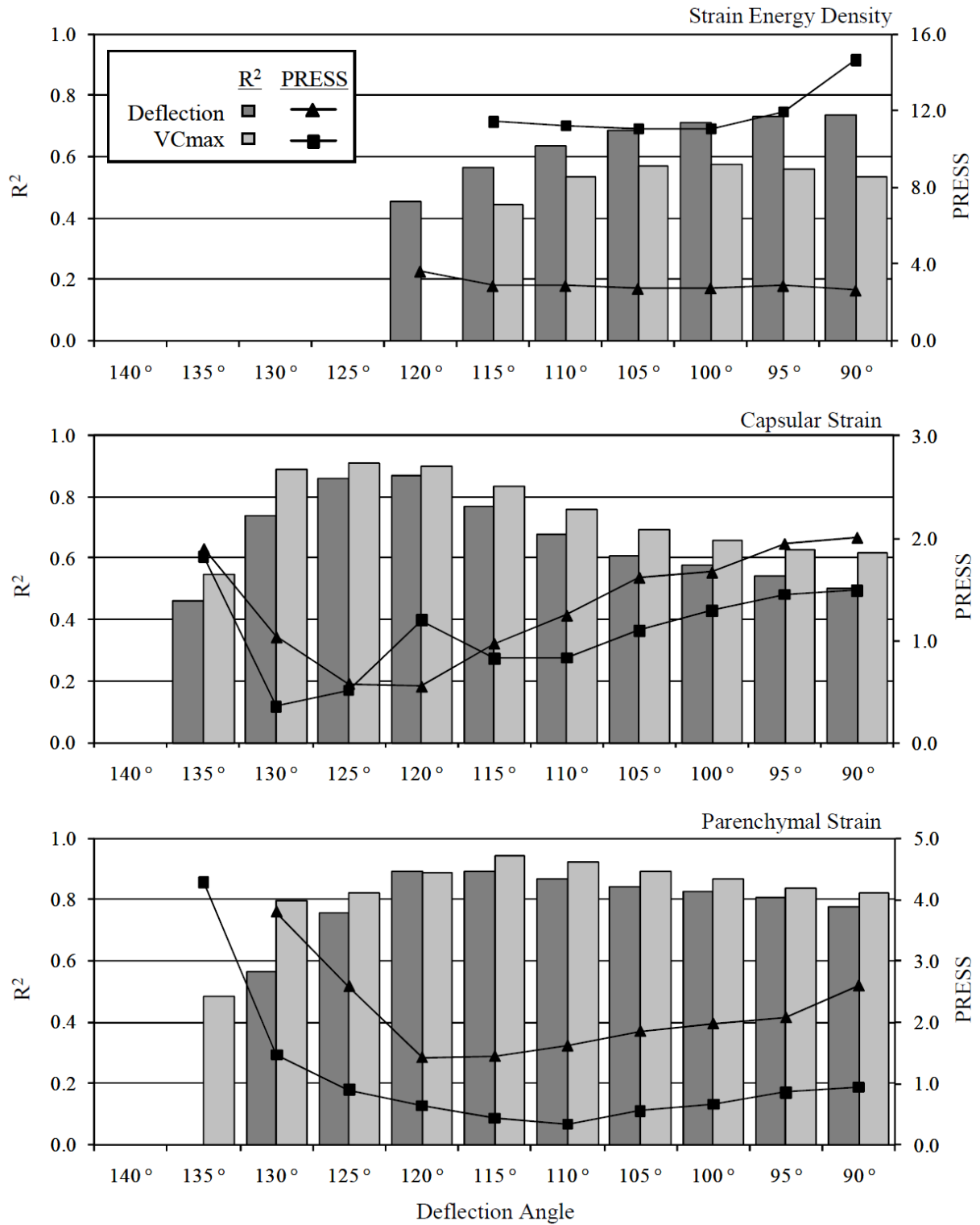


Figure 7. Coefficients of Determination (R^2) and PRESS statistics for correlations between oblique biomechanical parameters and tissue-level responses with large (95th percentile) viscera model.

Although a material response-based injury metric has not been developed for splenic trauma, parameters of parenchymal maximum principal strain, capsular strain, and strain energy density are mechanically justified. In the previous analysis, three of the four highest NRG, ϵ_C , and ϵ_1 values were obtained from chestband loadings which induced visceral injury in PMHS experiments (Hallman et al., 2011b). Logistic regression results indicated injury prediction with these material properties; p-values at or below $p = 0.1$ for each of the material responses (Hallman et al., 2011b). Material strain and rate-dependent strain energy density are important parameters of tissue failure in biological material trauma (Yamada, 1970). Trauma to renal capsule and parenchyma was correlated to maximum strain energy density in a viscoelastic finite element model of an *ex vivo* perfused porcine kidney (Snedeker et al., 2005, Snedeker et al., 2007). Derivations of maximum principal strain were correlated to neural trauma as identified by rodent unconscious time and histological evaluations (Fijalkowski et al., 2009). Maximum principal strain was correlated to lung contusion in blunt impacts to rodent subjects (Stitzel et al., 2005). The diversity of these tissues validated the extension of response criteria to spleen tissue. Rib fracture was not considered by the model. Rather, the generalized chest wall material was linearly elastic without failure. Rib fractures have been considered by element erosion (deletion) with failure strain value (Hayashi et al., 2008; Song et al., 2009). Yet component analysis and pendulum validation have demonstrated the present formulation to be sufficiently physiologic for this analysis (Hallman et al., 2011b).

Visceral geometry was a determinant of the level of external biomechanical correlation. Comparing PRESS and R^2 values, material responses in the small viscera model correlated poorly in comparison to the other geometries. Highest overall R^2 values occurred in the large viscera model. For this anatomic variant, VCmax was a better predictor of maximum parenchymal and capsular strain than normalized deflection. In the median viscera model normalized deflection was preferable for ϵ_1 and ϵ_C . Clinical evidence has suggested that splenomegaly and hepatomegaly may be associated with increased risk of trauma (Arden et al., 1981). Therefore, the large anatomic variant may be more relevant to injury risk determination using an ATD, suggesting that VCmax is most appropriate. Yet observed injury patterns (Hallman et al., 2010) were limited to normophysiologic specimens which may be more indicative of median anatomic variants. Therefore results suggested that normalized deflection and VCmax should be used concurrently in injury risk assessments. These parameters should be obtained from angles between $\theta = 115^\circ - 125^\circ$ with respect to the anterior direction.

Clinical data has associated acute splenomegaly with increased risk of splenic rupture, particularly during infection (Putukian et al., 2008). The large spleen model in this study was associated with increased parenchymal and capsular strain as well as increased strain energy density. Yet cases of chronic splenomegaly have not been associated with increased risk of trauma (Pottakkat et al., 2006), possibly due to fibrotic changes in splenic tissue composition. To address such material changes, a sensitivity analysis was conducted which examined the relationship between material responses (ϵ_1 , NRG, and ϵ_C) and splenic tissue material properties (Table 1). The chestband loading chosen for this sensitivity analysis corresponded to the most severe splenic trauma case. Spleen parenchymal tissue properties of density (ρ), bulk modulus (K), and shear moduli (G_0 and G_∞) were arbitrarily varied by 50% ($\pm 25\%$). Results of this analysis are shown in Figure 8. All material response parameters were most sensitive to K, a finding in agreement with the literature (Shen et al., 2008). Strain energy density was highly sensitive to ρ , but this was due primarily to the derivation of this response parameter. Increased G_0 and G_∞ induced increases in capsular strain and decreases in parenchymal strain. In light of this analysis, material property changes induced by chronic splenomegaly likely included increased shear and bulk moduli. Splenic capsular material changes were not addressed by this analysis but likely include similar fibrotic stiffening. Computational analysis has suggested a stiffening relationship between biological tissue perfusion and material bulk response (Bilston, 2002). Therefore during acute splenomegaly, capsular material changes would be unlikely, but inflammation may increase the parenchymal bulk modulus (K), elevating both capsular and parenchymal strains.

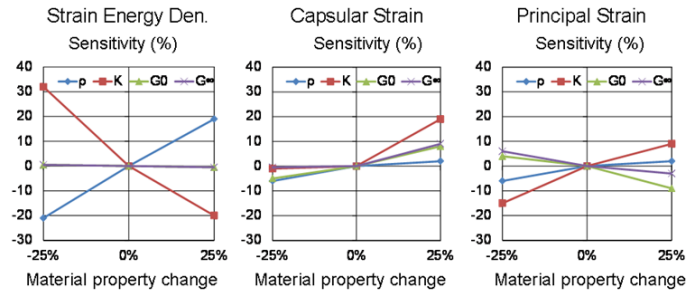


Figure 8. Maximum material response sensitivity to spleen parenchymal tissue properties.

Few analyses have addressed biomechanical and injury response to posterolateral loading of the thorax or abdomen. One study varied impact angle to 105° with respect to anterior for anthropomorphic test device validation and quantified only spinal accelerations (Morgan & Waters, 1980). A more recent study addressed similar objectives but quantified deflection and stiffness at 105° (Subit et al., 2010). Similarly, crashes resulting in 4 - 5 or 7 - 8 o'clock principal directions of force are rarer than other lateral impact variants (Dischinger et al., 1993). Therefore, the side airbag loading utilized in the present study may represent a common posterolateral thoracic and abdominal loading mechanism in the contemporary vehicle fleet.

The model did not differentiate between peak deflection and VCmax as predictors of visceral injury. These results are consistent with cadaveric experiments (Hallman, 2010). This suggested that, for this posterolateral boundary condition, both are appropriate. A study of anterior PMHS loading reported a similar conclusion (Kent et al., 2001). Specifically, it was observed that VCmax injury criteria (thresholds) were exceeded in conjunction with normalized deflection criteria in all dynamic loading scenarios. Therefore, as current procedures suggest that both metrics be quantified in vehicle crashworthiness assessments, these results support such a practice.

The limitations of this study include the plane strain model formulation. This formulation constrained element deformations to planar response only. This approach has been employed previously for computational examination of thoracoabdominal injury response with chestband contours (Campbell et al., 2005). Further, the homogenous treatment of splenic tissue in this study did not consider devascularization injuries seen clinically (Madoff et al., 2005). Yet devascularization is rare in absence of other parenchymal damage to which the model composition was sensitive (Arden et al., 1981). Similarly, rib fracture was not considered by the elastic chest wall model. This injury pattern, although present in PMHS subjects, was not necessarily unique to the boundary condition, and visceral shearing by fractured rib ends represents a self-evident injury mechanism. Finally, as with all computational models of trauma, assumption with regard to material models may affect results. Complex nonlinear tissues were assumed to be linear elastic and viscoelastic materials such that study aims were achievable. Previous studies have suggested linear viscoelasticity and elasticity to represent an appropriate material model for impact (Shen et al., 2008; Fijalkowski et al., 2009).

CONCLUSIONS

A planar viscoelastic finite element model was coupled to subject-specific chestband contours to evaluate metric and measurement direction most correlated to internal tissue response. This study suggested that normalized deflection and VCmax should be used concurrently in injury risk assessments. These parameters should be obtained from angles between $\theta = 115^\circ - 125^\circ$ with respect to the anterior direction.

ACKNOWLEDGMENTS

This research was supported in part by the National Science Foundation Graduate Research Fellowship Program and Veterans Affairs Medical Research.

REFERENCES

- ARDEN, G. P., CHRISTIAN, M. S., & WILLIAMS, E. J. Traumatic rupture of the spleen. *International Journal of Surgery*, 66(2), 1981, 149-53.
- BEHR, M., ARNOUX, P. J., SERRE, T., BIDAL, S., KANG, H. S., THOLLON, L., CAVALLERO, C., KAYVANTASH, K., & BRUNET, C. A human model for road safety: From geometrical acquisition to model validation with radioss. *Computer Methods in Biomechanics & Biomedical Engineering*, 2003, 6(4), 263.
- BILSTON, L. E. The effect of perfusion on soft tissue mechanical properties: A computational model. *Computer Methods in Biomechanics and Biomedical Engineering*, 2002, 5(4), 283-290.
- CAMPBELL, J. Q., TANNOUS, R. E., TAKHOUNTS, E. G., MARTIN, P. G., EPPINGER, R. H., & NGUYEN, T. On the development of a theoretically based, statistically justified, thoracic injury criterion. *19th International Technical Conference on the Enhanced Safety of Vehicles*, Washington, DC. 2005.
- CARTER, F. J., FRANK, T. G., DAVIES, P. J., MCLEAN, D., & CUSCHIERI, A. Measurements and modelling of the compliance of human and porcine organs. *Medical Image Analysis*, 2001, 5(4), 231-236.
- CHUNG, J., CAVANAUGH, J. M., KING, A. I., KOH, S., & DENG, Y. C. Thoracic injury mechanisms and biomechanical responses in lateral velocity pulse impacts. *43rd Stapp Car Crash Conference*, San Diego, CA. 1999.
- DISCHENGER, P. C., CUSHING, B. M., & KERNS, T. J. Injury patterns associated with direction of impact: Drivers admitted to trauma centers. *Journal of Trauma*, 1993, 35(3), 454-9.
- EPPINGER, R. H. On the development of a deformation measurement system and its application toward developing mechanically based injury indices. *33rd Stapp Car Crash Conference*, Washington, DC. 1989. 21-28.
- GERAGHTY, E. M., BOONE, J. M., MCGAHAN, J. P., & JAIN, K. Normal organ volume assessment from abdominal CT. *Abdominal Imaging*, 2004, 29(4), 482-490.
- FIJALKOWSKI, R. J., YOGANANDAN, N., ZHANG, J., & PINTAR, F. A. A finite element model of region-specific response for mild diffuse brain injury. *Stapp Car Crash Journal*, 2009, 53, 193-213.
- HALLMAN, J. J. Detrimental thoracoabdominal interaction with lateral airbag restraints. Dissertation, Marquette University, 2010.
- HALLMAN, J. J., YOGANANDAN, N., & PINTAR, F. A. Biomechanical and injury response to posterolateral loading from torso side airbags. *Stapp Car Crash Journal*, 2010, 54, 227-257.
- HALLMAN, J. J., YOGANANDAN, N., & PINTAR, F. A. Technique for chestband contour shape-mapping in lateral impact. *Journal of Biomechanics*, 2011, 44(12), 2328-32.
- HALLMAN, J. J., YOGANANDAN, N., & PINTAR, F. A. Prediction of visceral response to multi-directional loading as measured by the chestband. *Medical Engineering and Physics*, 2011. doi: 10.1016/j.medengphy.2011.10.006
- HAYASHI, S., YASUKI, T., & KITAGAWA, Y. Occupant kinematics and estimated effectiveness of side airbags in pole side impacts using a human FE model with internal organs. *Stapp Car Crash Journal*, 2008, 52, 363-377.
- KEMPER, A. R., MCNALLY, C., KENNEDY, E. A., MANOOGIAN, S. J., & DUMA, S. M. The influence of arm position on thoracic response in side impacts. *Stapp Car Crash Journal*, 2008, 52, 379-420.
- KENT, R. W. Frontal thoracic response to dynamic loading: The role of superficial tissues, viscera and the rib cage. *International Journal of Crashworthiness*, 2008, 13(3), 289-300.
- KENT, R. W., CRANDALL, J. R., BOLTON, J., PRASAD, P., NUSHOLTZ, G., & MERTZ, H. The influence of superficial soft tissues and restraint condition on thoracic skeletal injury prediction. *Stapp Car Crash Journal*, 2001, 45, 183-204.

- KUPPA, S., EPPINGER, R. H., MCKOY, F., NGUYEN, T., PINTAR, F. A., & YOGANANDAN, N. Development of side impact thoracic injury criteria and their application to the modified ES-2 dummy with rib extensions (ES-2re). *Stapp Car Crash Journal*, 2003, 47, 189-210.
- MADOFF, D. C., DENYS, A., WALLACE, M. J., MURTHY, R., GUPTA, S., PILLSBURY, E. P., AHRAR, K., BESSOUD, B., & HICKS, M. E. Splenic arterial interventions: Anatomy, indications, technical considerations, and potential complications. *Radiographics*, 2005, 25, S191-S211.
- MELVIN, J. W., STALNAKER, R. L., ROBERTS, V. L., & TROLLOPE, M. L. Impact injury mechanisms in abdominal organs. *17th Stapp Car Crash Conference*, Oklahoma City, OK. 1973. 115-126.
- MOHR, M., ABRAMS, E., ENGEL, C., LONG, W. B., & BOTTLANG, M. Geometry of human ribs pertinent to orthopedic chest-wall reconstruction. *Journal of Biomechanics*, 2007, 40(6), 1310-1317.
- MORGAN, R. M. & WATERS, H. P. Comparison of two promising side impact dummies. *8th International Technical Conference on the Enhanced Safety of Vehicles*. Wolfsburg, Germany, 1980, 472-482.
- PINTAR, F. A., YOGANANDAN, N., SANCES, A., JR., & EPPINGER, R. H. Instrumentation of human surrogates for side impact. *40th Stapp Car Crash Conference*, Albuquerque, NM. 1996. 29-42.
- PINTAR, F. A., YOGANANDAN, N., HINES, M. H., MALTESE, M. R., MCFADDEN, J., SAUL, R., EPPINGER, R. H., KHAEWPOONG, N., & KLEINBERGER, M. Chestband analysis of human tolerance to side impact. *41st Stapp Car Crash Conference*, Lake Buena Vista, FL. 1997. 63-74.
- POTTOKKAT, B., KASHYAP, R., KUMAR, A., SIKORA, S. S., SAXENA, R., & KAPOOR, V. K. Redefining the role of splenectomy in patients with idiopathic splenomegaly. *ANZ Journal of Surgery*, 2006, 76(8), 679-682.
- PUTUKIAN, M., O'CONNOR, F. G., STRICKER, P., MCGREW, C., HOSEY, R. G., GORDON, S. M., KINDERKNECHT, J., KRISS, V., & LANDRY, G. Mononucleosis and athletic participation: An evidence-based subject review. *Clinical Journal of Sports Medicine*, 2008, 18(4), 309-315.
- RUAN, J., EL-JAWAHRI, R., CHAI, L., BARBAT, S., & PRASAD, P. Prediction and analysis of human thoracic impact responses and injuries in cadaver impacts using a full human body finite element model. *Stapp Car Crash Journal*, 2003, 47, 299-321.
- SCHNEIDER, L. W., ROBBINS, D. H., PFLUEG, M. A., & SNYDER, R. G. *Anthropometry of motor vehicle occupants*. Washington, DC: National Highway Traffic Safety Administration, 1985.
- SEKI, S., & IWAMOTO, H. Disruptive forces for swine heart, liver, and spleen: Their breaking stresses. *The Journal of Trauma*, 1998, 45(6), 1079-1083.
- SHAW, J. M., HERRIOTT, R. G., MCFADDEN, J. D., DONNELLY, B. R., & BOLTE, J. H., 4TH. Oblique and lateral impact response of the PMHS thorax. *Stapp Car Crash Journal*, 2006, 50, 147-167.
- SHEN, W., NIU, Y., MATTREY, R. F., FOURNIER, A., CORBEIL, J., KONO, Y., & STUHMILLER, J. H. Development and validation of subject-specific finite element models for blunt trauma study. *Journal of Biomechanical Engineering*, 2008, 130(2), 021022.
- SNEDEKER, J. G., BARBEZAT, M., NIEDERER, P., SCHMIDLIN, F. R., & FARSHAD, M. Strain energy density as a rupture criterion for the kidney: Impact tests on porcine organs, finite element simulation, and a baseline comparison between human and porcine tissues. *Journal of Biomechanics*, 2005, 38(5), 993-1001.
- SNEDEKER, J. G., BARNSTUBLE, B. B., IAIZZO, P. A., FARSHAD, M., NIEDERER, P., & SCHMIDLIN, F. R. A comprehensive renal injury concept based on a validated finite element model of the human abdomen. *The Journal of Trauma*, 2007, 62(5), 1240-1249.
- SONG, E., TROSSEILLE, X., & BAUDRIT, P. Evaluation of thoracic deflection as an injury criterion for side impact using a finite elements thorax model. *Stapp Car Crash Journal*, 2009, 53, 155-191.
- SPITZER, V., ACKERMAN, M. J., SCHERZINGER, A. L., & WHITLOCK, D. The visible human male: A technical report. *Journal of the American Medical Informatics Association : JAMIA*, 1996, 3(2), 118-130.

- STINGL, J., BACA, V., CECH, P., KOVANDA, J., KOVANDOVA, H., MANDYS, V., REJMONTOVA, J., & SOSNA, B. Morphology and some biomechanical properties of human liver and spleen. *Surgical and Radiologic Anatomy : SRA*, 2002, 24(5), 285-289.
- STITZEL, J. D., GAYZIK, F. S., HOTH, J. J., MERCIER, J., GAGE, H. D., MORTON, K. A., DUMA, S. M., & PAYNE, R. M. Development of a finite element-based injury metric for pulmonary contusion part I: Model development and validation. *Stapp Car Crash Journal*, 2005, 49, 271-289.
- SUBIT, D., DUREY, S., LAU, S., GUILLEMOT, H., LESSLEY, D., KENT, R. Response of the human torso to lateral and oblique constant-velocity impact. *Annals of Advances in Automotive Medicine*, 2010, 54, 027-40.
- TAMURA, A., OMORI, K., MIKI, K., LEE, J. B., YANG, K. H., & KING, A. I. Mechanical characterization of porcine abdominal organs. *Stapp Car Crash Journal*, 2002, 46, 55-69.
- VIANO, D. C., LAU, I. V., ANDRZEJAK, D. V., & ASBURY, C. Biomechanics of injury in lateral impacts. *Accident; Analysis and Prevention*, 1989, 21(6), 535-551.
- YAMADA, H. (1970). *Strength of biological materials*. Huntington, New York: Williams & Wilkins.
- YOGANANDAN, N., & PINTAR, F. A. Biomechanics of human thoracic ribs. *Journal of Biomechanical Engineering*, 1998, 120(1), 100-104.
- YOGANANDAN, N., PINTAR, F. A., GENNARELLI, T. A., MARTIN, P. G., & RIDELLA, S. A. Chest deflections and injuries in oblique lateral impacts. *Traffic Injury Prevention*, 2008, 9(2), 162-167.